Available online at www.sciencedirect.com
SCIENCE DIRECT
International Journal of Heat and Mass Transfer 49 (2006) 1667–1678
International Journal of HEAT and MASS TRANSFER
www.elsevier.com/locate/ijhmt

An experimental and numerical investigation of flow patterns in the entrance of plate-fin heat exchanger

Jian Wen *, Yanzhong Li *, Aimin Zhou, Ke Zhang

Department of Refrigeration and Cryogenics Engineering, School of Energy and Power Engineering, Xi'an Jiaotong University, Xi'an 710049, PR China

Received 17 May 2005; received in revised form 18 October 2005
Available online 19 January 2006

Abstract

The turbulent flow structure inside the entrance of plate-fin heat exchanger was characterized by CFD simulation and PIV experiment under the similar conditions. A series of velocity vectors and streamline graphs of different cross-sections are achieved for three distinct header configurations, involving conventional and improved configurations. The numerical and experimental results indicate that the performance of fluid maldistribution in conventional entrance is deteriorated, while the improved configuration with punched baffle can effectively improve the performance in both radial and axial direction. And the baffle on which the small holes are distributed in staggered arrangement is the first choice for the improvement. CFD results and PIV data are in good agreement with each other. The results validate that PIV and CFD are well suitable to investigate complex flow patterns and the conclusion of this paper is of great significance in the optimum design of plate-fin heat exchanger.

Keywords: Plate-fin heat exchanger; PIV; Numerical simulation; Optimum design

1. Introduction

Plate-fin heat exchangers are employed in a wide variety of engineering applications such as air separation and petrochemical industries to exchange heat energy among more than two-fluids with different supply temperatures because of their high efficiency, more compact structure and lower costs than two-stream heat exchanger networks [1–3]. The use of multi-stream plate-fin heat exchangers is more cost-effective and can offer significant advantages over conventional two-stream heat exchangers in certain applications, especially in cryogenic plants. The longitudinal wall heat conduction, the nonuniformity of temperature field and fluid flow could be coupled, which is the main reason that causes the deterioration of heat exchanger efficiency, especially for the compact heat exchanger [4]. The effect of fluid flow nonuniformity on heat exchanger efficiency is of first-order importance because it can intensify longitudinal wall heat conduction and the maldistribution of interior temperature. The flow nonuniformity through the exchanger is generally associated with improper exchanger entrance configuration—poor header design and imperfect passage-to-passage flow distribution in a highly compact heat exchanger caused by various manufacturing tolerances.

The flow nonuniformity effects have been well recognized and presented for heat exchangers in recent years. Most of previous works mainly investigated the effect of flow nonuniformity on the heat exchangers performance deterioration based on their own flow maldistribution model. Ranganayakulu et al. [5] investigated the effect of two-dimensional nonuniform inlet fluid flow distribution on both hot and cold fluid sides of cross-flow plate-fin heat exchanger using a finite element model. And it was found that the performance deteriorations and variation in pressure drops are quite significant in some typical applications

* Corresponding authors. Tel.: +86 29 82663725; fax: +86 29 82668725 (J. Wen), Tel.: +86 29 82668725; fax: +86 29 82668789 (Y. Li).
E-mail addresses: wenjian@mailst.xjtu.edu.cn (J. Wen), yzli-epe@mail.xjtu.edu.cn (Y. Li).

0017-9310/$ - see front matter © 2005 Elsevier Ltd. All rights reserved.
doi:10.1016/j.ijheatmasstransfer.2005.10.029

Nomenclature

k	turbulent kinetic energy (m^2/s^2)
L	the length of header (mm)
N	the number of channels/measuring point
r	radius of the header cylinder (mm)
R	radius of small holes (mm)
Re	Reynolds number
S	flow maldistribution parameter
S_g	global flow maldistribution parameter
S_l	local flow maldistribution parameter
s_Φ	source term for generalized variable Φ
T	temperature (°C)
U	velocity (m/s)
u	velocity component in x-direction (m/s)
v	fluid flow rate/velocity component in y-direction (m/s)

Greek symbols

ε	turbulent energy dissipation rate (m^2/s^3)
Γ	effective diffusivity (m^2/s)
ρ	density of the fluid (kg/m^3)
Φ	generalized notation for transport variable
θ	velocity ratio
δ	relative standard deviation

Subscripts

ave	average value
c	cold fluid
h	hot fluid
i	serial number of passage/coordinate in x-direction
in	inlet
j	coordinate in y-direction
k	frame number in PIV measurement
max	maximum value
min	minimum value

due to fluid flow nonuniformity. Fleming [6] set up a flow maldistribution model in paired-channel heat exchangers and investigated the effect of flow maldistribution on the performance deterioration. Chiou [7] set up a continuous flow distribution model and studied the thermal performance deterioration in cross-flow heat exchangers. Axial temperature profiles in a shell and tube heat exchanger were numerically calculated for given maldistributions on the tube side by Roetzel and Ranong [8]. In fact, a flow distribution model that can precisely describe the real flow distribution in plate-fin heat exchanger does not exist. A few literatures of experimental investigation on flow maldistribution in plate heat exchangers can be found in these years. Lalot et al. [9] etc. investigated the effect of flow nonuniformity on the performance of plate heat exchangers. They also found the optimum location of perforated grid in header and reverse flow could occur with poor inlet header design. The literature of improved configuration to enhance the flow uniformity in plate-fin heat exchanger is limited in recent years. Jiao et al. [10] investigated experimentally and analyzed theoretically the combined effects of distributors' inlet angle and header configuration on flow velocity distribution. Zhang and Li [11] proposed a structure of two-stage-distribution and the numerical investigation shows the flow distribution in plate-fin heat exchanger is more uniform if the ratio of outlet and inlet equivalent diameters for both headers is equal.

PIV is an instantaneous whole-field measurement technique, which uses a pulsed light-sheet to illuminate a gas flow seeded with tracer particles. Four to six successive image of the tracer particles are recorded photographically and the pictures digitized. It can potentially provide more information about flow mechanism than that from conventional measurement techniques. PIV has already had quite a lot of applications in studies of fluid mechanics, marine hydrodynamics and aerodynamics [12–15]. It has broken through some limitations of single point measurement of conventional measuring technology. It is able not merely to measure the instantaneous velocity field of fluid from low-speed to supersonic range, but also succeeds in applying to the measurement of multiphase flow, thermo-fluid and turbulent structures, etc. So PIV technology is used to study the characters of fluid distribution in the header of plate-fin heat exchangers in this paper.

To study the effects of entrance configuration on fluid flow maldistribution is very important for the optimum of configuration and making the fluid flow more uniform in heat exchangers. So this research is valuable in academics and engineering. On the basis of numerical simulation [16], improved header configuration with punched baffle is proposed in this paper. The flow characteristics of flow field in the header of plate-fin heat exchanger have been investigated by means of computational fluid dynamics (CFD) and Particle Image Velocimetry (PIV), which are performed under similar conditions. A series of velocity vectors and streamline graphs at different cross-sections are achieved in CFD simulation and PIV experiment to get better header configuration.

2. Numerical model

2.1. The physical model

A schematic view of conventional header (denoted as configuration A) is shown in Fig. 1, which has the geometrical characteristics listed as follows. The diameter of the

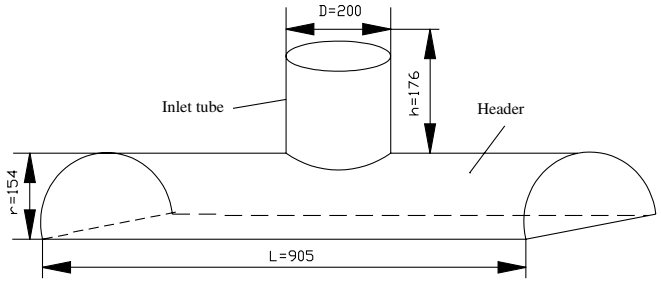

Fig. 1. Model of header construction.

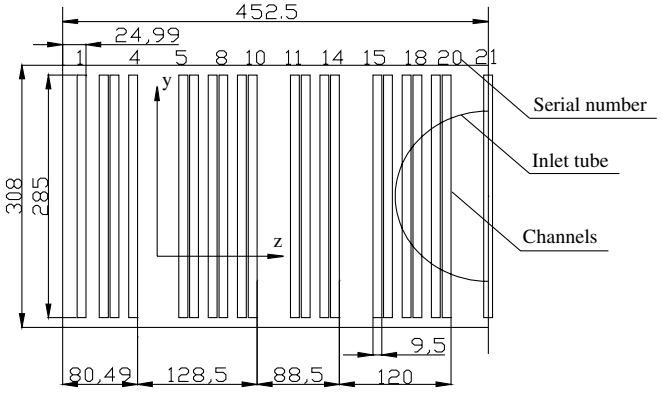

Fig. 2. Definition of the channels at the outlet of header.

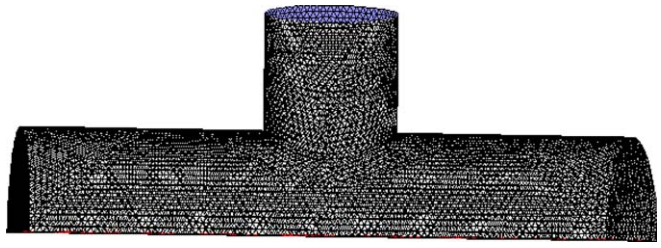

Fig. 3. Finest mesh implement using Gambit.

inlet flow pipe is equal to 200 mm, the radius of the header is 154 mm and it is 905 mm in length, which are all the same with actual dimensions. Fig. 2 shows the definition of channels at the outlet of half the header length for the structural symmetry (The labeled serial number in the figure indicates the location of test cross-section in PIV experiment). Composite constructive grids are used in the analog computation and the finest implemented grid involved about 245,817 cells (Fig. 3). There are selective refined grids in some local place where parametric variation is severe.

2.2. The mathematic model

There are some assumptions in the CFD simulation: (1) the flow is stable in the test section; (2) the fluid flow meets the Boussinesq assumption and (3) the fluid in the test section is incompressible Newtonian fluid.

In this work, CFD software FLUENT was employed to simulate the fluid flow distribution in the header of plate-fin heat exchanger. FLUENT is one of the most widely used commercial codes for simulating engineering fluid flow due to its accuracy, robustness and convenience. In FLUENT, the conservation equations of mass, momentum are solved using the finite volume method. There are several turbulence models available in the code. The turbulence flow was calculated by the Semi-implicit SIMPLER Algorithm method in the velocity and pressure conjugated problem, and a second order upwind differential scheme was applied for the approximation of the convective terms.

A standard k–ε model was used to predict turbulent flow in the header. The Reynolds transport equations in all the three directions and the 'k' and 'ε' equations can be written in a generalized form as [17,18]:

$$\frac{\partial(\rho u\Phi)}{\partial x}+\frac{1}{r}\frac{\partial(r\rho v\Phi)}{\partial r}+\frac{1}{r}\frac{\partial(\rho w\Phi)}{\partial\theta} = \frac{\partial}{\partial x}\left(\Gamma\frac{\partial\Phi}{\partial x}\right)+\frac{1}{r}\frac{\partial}{\partial r}\left(\Gamma r\frac{\partial\Phi}{\partial r}\right)+\frac{1}{r}\frac{\partial}{\partial\theta}\left(\frac{\Gamma}{r}\frac{\partial\Phi}{\partial\theta}\right)+s_\Phi \quad (1)$$

where Φ stands for a generalized transport variable, which is used for all conserved variables in a fluid flow problem, including mass, momentum, and the turbulence variables k and ε. Γ represents the effective diffusivity (sum of the eddy diffusivity and the molecular diffusivity). s_Φ is the source term for the respective dependent variable. The value of source term s_Φ depends on the respective type of Φ. The solution of the above set of equations was applied to the prediction of velocity and turbulence levels throughout the header.

Boundary conditions and convergent condition are as follows: Inlet fluid velocity and temperature are given, and the pressure at outlet vent is specified. Adiabatic wall condition is applied and no slip occurs at the wall. Convergent criterion is specified to absolute residuals $\leqslant 1.0\times10^{-6}$.

3. Experimental setup and approach

3.1. Experimental system

Fig. 4 shows the schematic drawing of experimental system, which consists of wind path system and PIV system. And the arrangement of them is also illustrated in the diagram.

In the wind path system, the air is supplied by a upstream fan and the flux is measured by an orifice flow meter installed in the pipeline. The pressure difference is measured by U-shaped tube. Water is adopted as the working fluid and the minimum scale of the U-shaped tube is 1 mm. Among the measurement range, the relative error of the pressure difference is less than 1%. There are pipes with the same diameter as stable pipeline in the upstream and downstream of the orifice respectively, which not merely benefit the measurement of the flow, but also make the fluid distributed more uniformly at the inlet of header.

The measurement of the velocity field in the header was carried out with a two-dimensional PIV equipment, which consists of illumination system, image acquisition system,

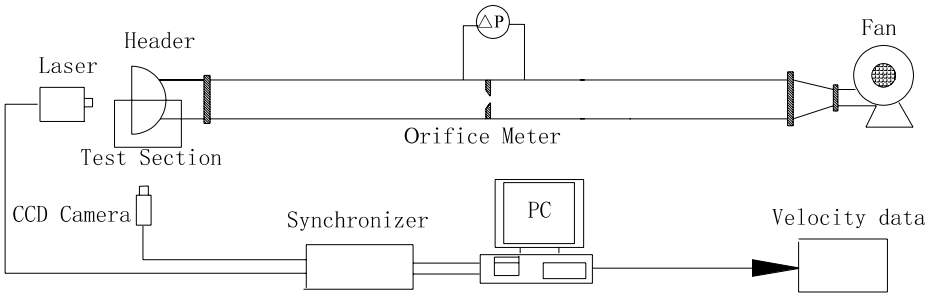

Fig. 4. Schematic diagram of experimental system.

synchronous controlling system and image processing system. Light source is supplied by a large power harmonic Nd-YAG twin laser system (wavelength $\lambda = 532$ mm, pulse energy = 50 MJ). The pulsed laser and the light-sheet optics are part of the illumination system. The light-sheet optics includes cylindrical and spherical lenses. The cylindrical lens diverges the laser beam in one direction but keeps it the same thickness as the laser beam in the other direction. This gives light-sheet some height but which is still thin. The spherical lens controls the light-sheet thickness. For the measurements, a light-sheet thickness of less than 1 mm is desired. The spherical lens creates a beam waist at its focal distance. Moving away from the focal distance the light-sheet is thicker. With the proper selection of light-sheet optics the laser light-sheet can be set to the correct size for experiment. The flow in a PIV experiment is illuminated with the pulsed laser light-sheet of a thickness of 1 mm. The camera is usually focused near the light-sheet waist, at the focal length of the spherical lens. The image signal acquisition is carried out by PIVCAM-30 of type 630046, whose resolution factor is 1018×1018 *pixel*. The fastest acquisition speed is 30 frames per second. The CCD camera is a combination of cross-frame and rapid-output of image signal matrix that enable to capture two images with minimum time separation of 1 μs. Synchronizer is used to control the output of laser pulse and the sequence of image acquisition, which guarantees that all parts are coordinated and gone on according to the regular order. The software of controlling PIV system and data analysis is Insight NT. It can capture 1000 frame pictures in succession. 2-Frame Cross-Correlation and Fast Fourier Transforms are adopted in the data processing. Instantaneous velocity vector field and some other parameters distribution can also be obtained swiftly through batch processing.

The selection and seeding of tracer particles is one of the key factors of success or failure for PIV system measurement, especially for the case where air is adopted as the working fluid. Accompanying characteristic, scattering characteristic and uniformly sowing are the three aspects that the tracer particles should be considered of at the same time. The density of tracer particles should be proper in order to realize the flow field measurement by particle image. That is to say, the number of tracer particles should be abundant, but limited not to form scattered spots within certain area of the measured velocity field. In this experiment, Rosco1600 fog generator is used to generate tracer particles and fuming liquid especially used for air system is supplied by TSI Ltd. The average diameter of spherical drops is between 1 and 2 μm, which meets the demands of PIV system for tracer particles. In order to ensure the uniform scattering of tracer particles and reduce their interference to original flow field, the seeding of tracer particles is performed at the fan inlet, which is far away from the test area. Thus, tracer particles and inlet air enter the pipeline at the same time and have a uniform mixing at the test section.

3.2. The uncertainty of velocity measured by PIV

For each test cross-section, 200 frames of transient velocity field are obtained in the experiment. The time averaged velocity field of each test cross-section is then obtained through batch processing. The time average value of velocity components is as follows:

$$\bar{u}_{i,j} = \frac{\sum_{k=1}^{200} u_{i,j,k}}{200} \tag{2}$$

$$\bar{v}_{i,j} = \frac{\sum_{k=1}^{200} v_{i,j,k}}{200} \tag{3}$$

then the standard deviation value of velocity components is defined as

$$\Delta u_{i,j} = \sqrt{\frac{\sum_{k=1}^{200} \left(u_{i,j,k} - \bar{u}_{i,j}\right)^2}{199}} \tag{4}$$

$$\Delta v_{i,j} = \sqrt{\frac{\sum_{k=1}^{200} \left(v_{i,j,k} - \bar{v}_{i,j}\right)^2}{199}} \tag{5}$$

So the relative standard deviation of time average velocity is obtained

$$\delta U = \frac{\sqrt{\Delta u_{i,j}^2 + \Delta v_{i,j}^2}}{\sqrt{\bar{u}_{i,j}^2 + \bar{v}_{i,j}^2}} \tag{6}$$

$u_{i,j,k}$ is denoted as the x-direction velocity component of measuring point (i,j) in frame k. $v_{i,j,k}$ is denoted as the y-direction velocity component of measuring point (i,j) in frame k. With the proper matching of experimental parameter (such as the selection of cylindrical and spherical lenses

and so on), the relative measuring error of transient velocity field is limited not to exceed 1%. The relative standard deviation of time average velocity δU is less than 3.5% in the experiment.

3.3. Header configurations

The experimental model used in PIV experiment must be made of transparent materials in order to let the laser sheet illuminate the whole test cross-section and help CCD camera to capture the pictures. So all the test samples are made of lucite according to the original size, guaranteeing the performance of the prototype can be reflected as accurate as possible in the PIV experiment.

It has been found that the best position for the punched baffle is located in the midway between the inlet tube and the core of the header [9]. So a baffle with small holes is put forward to install at the 1/2 height of the header symmetrically, which is demonstrated in Fig. 5. The small holes are spotted in the baffle according to the velocity distribution of conventional header (denoted as configuration A) of CFD simulation and the punched ratio is gradually increasing in symmetry from the central axis to the boundary [16]. Three different kinds of holes in diameter are punched on the different baffle configurations. There are spotted symmetrically small ($2R = 10$ mm), medium ($2R = 20$ mm) and big ($2R = 30$ mm) holes from the axial line to the boundary on the baffle. And the punched zone of the small-size holes ($2R = 10$ mm) is the center where it is corresponding to the cross-section of the inlet flow pipe. The baffle shown in Fig. 6 (denoted as configuration B) has the dimension of $600 \times 260 \times 5$ mm^3 (length × width × thickness), and the holes are distributed with in-line arrangement. The dimension of baffle shown in Fig. 7

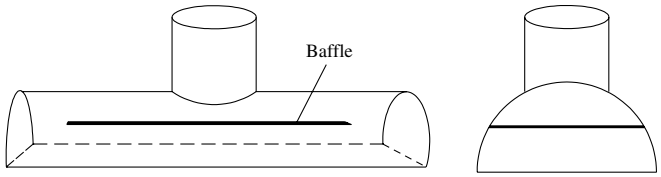

Fig. 5. Definition of the baffle position in the header.

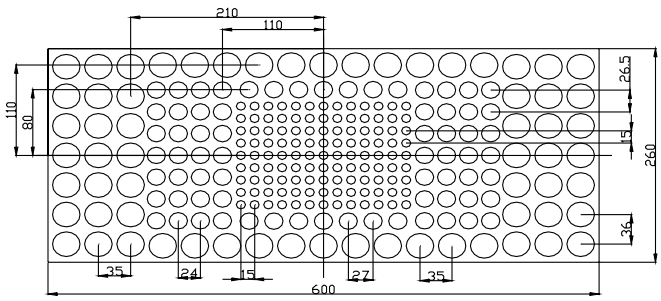

Fig. 6. Schematic drawing of baffle construction of configuration B.

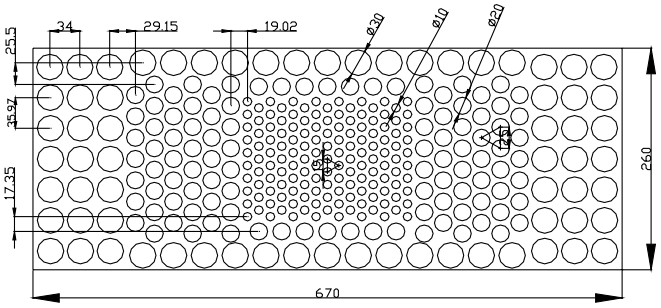

Fig. 7. Schematic drawing of baffle construction of configuration C.

(denoted as configuration C) is $670 \times 260 \times 5$ mm^3 (length × width × thickness). The small holes are distributed in staggered arrangement. There are conduit ferrules with the same baffle length at the 1/2 height of the header for the installation and fixation of punched baffles.

3.4. The selection of test cross-section

Because the physical dimension of the model is large, the pulsed laser light-sheet is not able to illuminate the whole test section. And the area of measured velocity field captured by CCD camera is limited to 150×150 mm. Due to the limitation of the laser light-sheet width and the minimum object size that the CCD camera can capture, also considering the symmetry of the header configuration, half the header cross-section is chosen as the measuring section (shown in Fig. 4). Fluid distribution conditions of different cross-sections along the direction of header length (z-direction) are measured by PIV system in the experiment.

Since the symmetry of header configuration exists, half the header length is measured in the PIV experiment. 11 cross-sections are measured from the central axis to the end boundary along the direction of header length (the labeled serial number in Fig. 2). The flow fields of three typical cross-sections are analyzed in the paper as illustrated in Fig. 8. Cross-section 1 is located at the central axis (channel 21 of Fig. 2), straightly facing the inlet tube. Cross-section 2 (channel 10 of Fig. 2) is deviated from

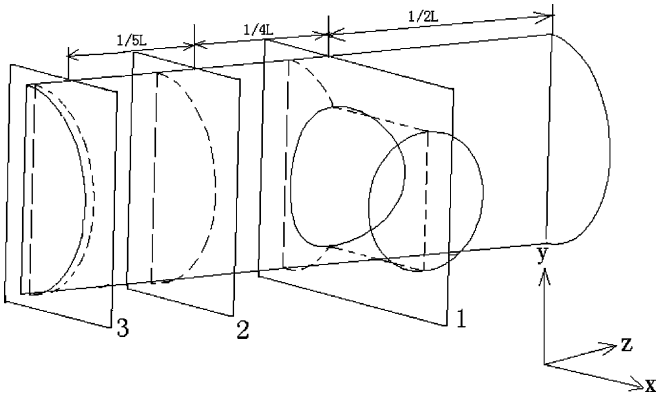

Fig. 8. Schematic diagram of test section location.

the inlet tube. And cross-section 3 (channel 1 of Fig. 2) is in the outer end of header and is the farthest away from the central axis of header.

3.5. Evaluation of flow maldistribution

Three parameters are introduced in this paper to evaluate the flow maldistribution, namely, global flow maldistribution parameter S_g, local flow maldistribution parameter S_l and velocity ratio θ, which are defined as follows:

$$S_{g,l} = \sqrt{\frac{1}{N-1}\sum_{i=1}^{N}(v_i - v_{ave})^2} \tag{7}$$

$$\theta = \frac{v_{max}}{v_{min}} \tag{8}$$

They disclose the dispersion degree of numerical and experimental results and reflect the flow maldistribution under different working conditions, different kinds of header configuration parameters and so on. The smaller the absolute value is, the more uniform the distribution is. For global flow maldistribution parameter S_g, N stands for the channel number (As shown in Fig. 2, 11 cross-sections are measured in the PIV experiment and the header configuration is symmetrical. So it is presumed that fluid in the header is distributed symmetrically and then the channel number is 21.), v_i stands for the average outlet velocity of each channel and v_{ave} stands for the average outlet velocity of all the channels. For local flow maldistribution S_l, N is defines as the number of measuring point with the same interval chosen along the y-direction in each cross-section and is equal to 20. v_i is the outlet velocity of measuring point *i chosen above*. v_{ave} stands for the average outlet velocity of each channel. v_{max} and v_{min} are the maximum velocity and minimum velocity of all the passages, respectively.

4. Results and discussion

The turbulent flow structure inside the entrance of plate-fin heat exchanger of different cross-sections was characterized using numerical simulations and PIV experiment. The computation and experiment are performed under the similar inlet Reynolds number ($Re = 6.0 \times 10^4$).

4.1. The results of conventional header configuration (configuration A)

Cross-section 1 shown in Fig. 9 is located at the central axis and facing the inlet tube. The figure (a) in left hand is obtained by CFD simulation and the figure (b) in right hand is got through PIV experiment. The flow maldistribution is very serious in the y-direction of the cross-section. The velocity is high and the upstream streamlines flow to the export in parallel, where the spot is facing the inlet tube of header in y-direction. While at the spot which is deviated from the inlet tube, fluid mainly flows from upstream and vortex is generated. A dead zone is formed for the reverse flow, thus fluid is distributed very nonuniformly in y-direction. It is because of the suddenly enlargement of fluid boundary geometry that flow behavior varies rapidly and the main flow separates from the surface to form vortex. The vortex can result in the loss of mechanical energy by converting into thermal energy. There is also mass transfer between the vortex and the main stream besides friction, so the energy loss is much. Because the inlet tube of header configuration is curved and too thick to fit for the observation of PIV experiment, so the area of observed cross-section is smaller compared with that of numerical simulation.

The cross-section 2 (shown in Fig. 10) is deviated from the inlet tube. As the distance from the inlet tube increases, small vortex enlarges gradually into large-scale vortex. So it can be concluded that fluid of this portion in the header are mainly distributed by the diffusion of vortex. It is because that fluid flows to the two sides of the header by

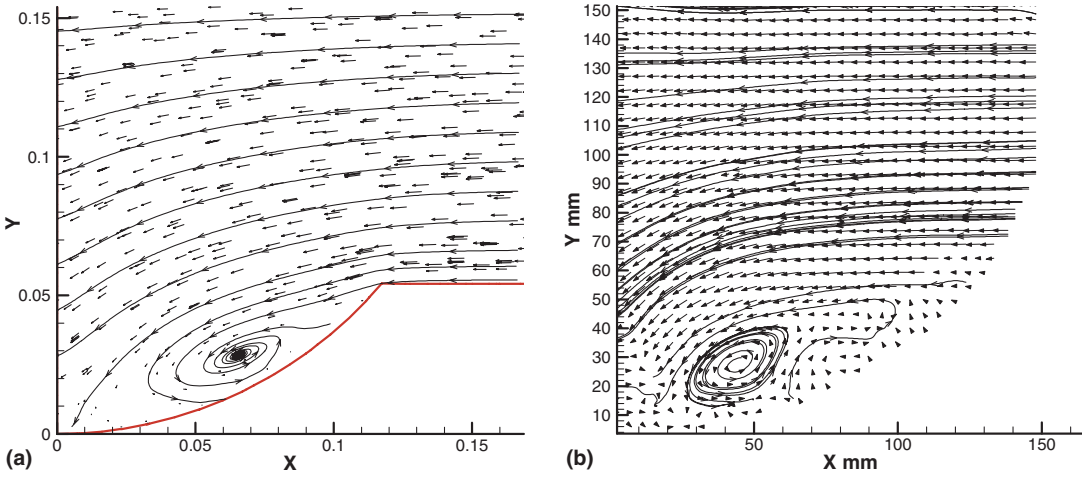

Fig. 9. The velocity vector and streamlines of cross-section 1 (configuration A): (a) CFD results (b) PIV results.

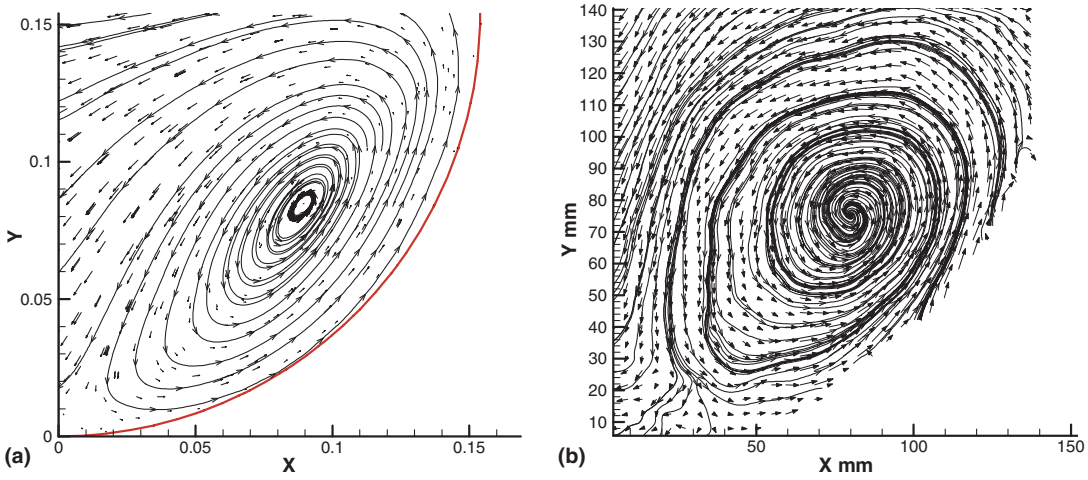

Fig. 10. The velocity vector and streamlines of cross-section 2 (configuration A): (a) CFD results and (b) PIV results.

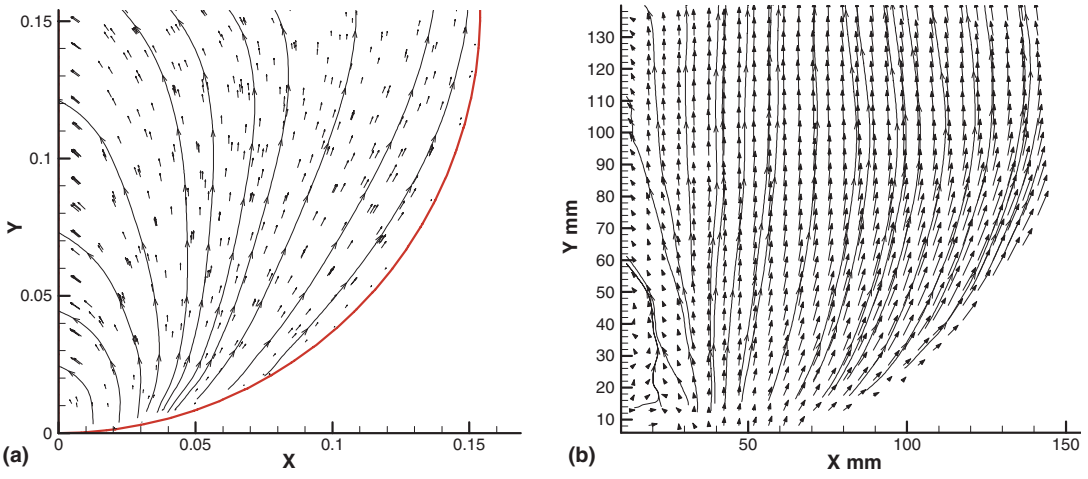

Fig. 11. The velocity vector and streamlines of cross-section 3 (configuration A): (a) CFD results and (b) PIV results.

the transverse pressure gradient at the outlet cross-section. Minority of the fluid reaches micro-channels and goes through, while the majority impacts on the boundary and is blocked. The fluid separates from the surface to form vortex and diffuses all around. And as the distance from the inlet tube further increases, the vortex may vanish for the viscous dissipation with all around fluid.

The cross-section 3 illustrated in Fig. 11 is at the boundary of the header and is the farthest away from the inlet tube. The majority of fluid has been branched off before it reaches the section and fluid kinetic energy is consumed by vortex, which results in the decrease of fluid velocity. So the fluid flux through the micro-channels nearby is very low and the section becomes the low speed zone of the header. And for the viscous dissipation between the fluid and the boundary, vortex vanishes and the streamlines are parallel to the outlet micro-channels.

Based on the analytical investigations of numerical and experimental results presented above, it can be concluded that it is mainly the fluid vortex and transverse pressure gradient that result in the fluid distribution in the conventional header. Thus the velocity near the inlet tube is high, while the velocity is low at the perimeter. Besides the fluid distribution nonuniformly, the energy loss caused by the vortex is high. So the header configuration should be improved to make the fluid distributed more uniformly.

4.2. The results of improved header configuration (configuration C)

The fluid from the inlet tube flows in front of the punched baffle. The circulation area expands suddenly and it causes the pressure reduction. Two kinds of factors cause the pressure drop, one is the irreversible effect, the other is the velocity variation. There are two kinds of condition that fluid reaches the baffle: (1) fluid reaches the small holes and goes through directly, which is the throttling expansion and (2) fluid reaches the baffle wall and is blocked. According to the Bernoulli equation, pressure rises and transverse pressure gradient is formed, which

results in fluid flowing all around and going through other small holes. And the different diameters of small holes are of great benefit to fluid uniform distribution. The small-size holes in the center part reduce the flux going through from the micro-channels adjacent to the central line. And the medium-size and large-size holes augment the flux that flows from the two side micro-channels. Thus the fluid is distributed evenly before it reaches the header outlet.

As shown in Fig. 12, the fluid is distributed more uniformly in y-direction and the dead zone vanishes in the cross-section 1 with the addition of punched baffle. In y-direction, the velocity facing the inlet tube decreases significantly, while that deviated from the inlet tube increases, comparing to that of configuration A. The diameter of small holes is the smallest in the center of the baffle, which creates much resistance to the fluid and transverse pressure gradient is formed to oblige fluid flow all around. While the diameter of the holes at the edge of the baffle is bigger and branch fluid can get through with no trouble. So the fluid of these cross-sections is distributed more uniformly in the y-direction. And the vortex in front of the punched baffle vanishes compared to that of conventional header configuration A. That is because the addition of baffle, which halves the header height and the space is too narrow to form vortex. In the experimental results, there are some vortices behind the punched baffle, facing the small holes. That is because the velocity of the fluid increases after going through the small holes and it initiates viscous shear with around low-speed fluid, so the vortexes are formed. While there is no small vortex in the numerical results for that the velocity at the solid wall was set to zero because of the utilization of the wall functions (such as no slip and no penetration) in the numerical simulation.

The cross-section 2 in Fig. 13 is deviated from the inlet tube. There is a big vortex in front of the baffle and the fluid is distributed uniformly after going through the baffle. Fluid from upstream is obstructed by the header wall and separates from the surface, thus an obvious vortex creates.

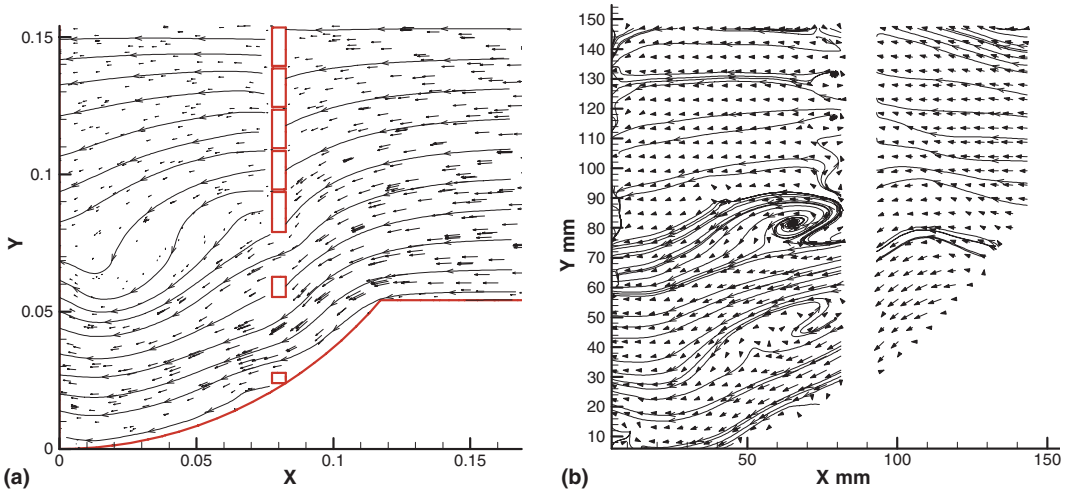

Fig. 12. The velocity vector and streamlines of cross-section 1 (configuration C): (a) CFD results and (b) PIV results.

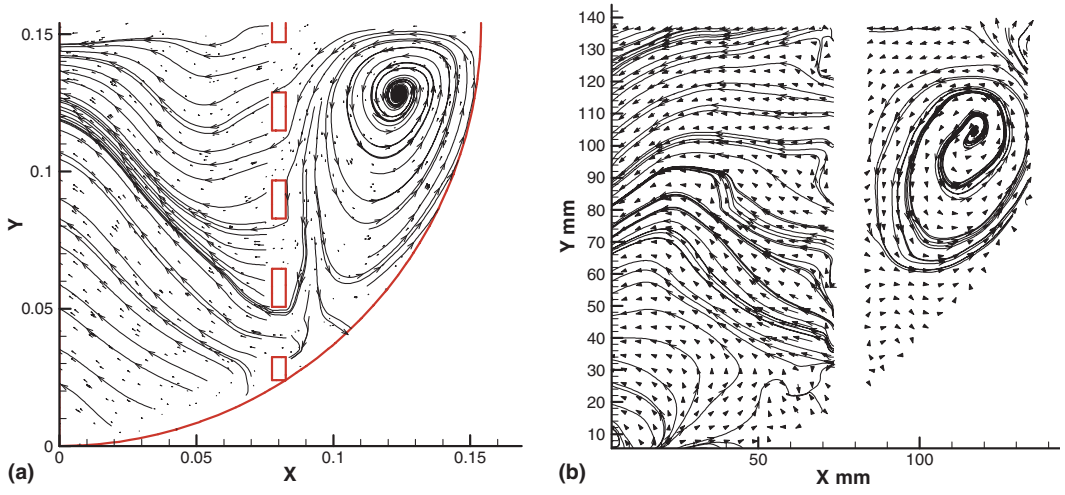

Fig. 13. The velocity vector and streamlines of cross-section 2 (configuration C): (a) CFD results and (b) PIV results.

For the cross-section does not face the inlet tube, so there are only medium-size and big-size holes in the punched baffle. Thus the resistance of baffle to fluid is low and the fluid is easy to go through. And fluid is distributed more uniformly after branched off by the small holes in the baffle.

As illustrated in Fig. 14, the velocities in cross-section 3 increase and the uniformity of fluid distribution is also improved greatly after the addition of the punched baffle. The streamlines are perpendicular to the outlet micro-channels. And fluid goes through the micro-channels directly. The vortex vanishes for the viscous dissipation with around low speed fluid. For the resistance of baffle wall, all the fluid going through from the baffle is less comparing to that of conventional header configuration A, which results in more fluid flowing from the cross-section and the velocities increase. That is to say, the fluid is distributed more uniformly for the increase of flux far away from the center axis with the addition of punched baffle.

The results of simulation and experiment illustrate that the fluid is distributed more uniformly. With the addition of punched baffle, fluid is distributed by the baffle and then flows to the header outlet. Not only in the axial direction, but also in the y-direction, the condition of fluid distribution is improved greatly. The number of big vortex decreases compared to that of conventional header configuration A. So the energy loss caused by turbulent dissipation reduces, which can compensates for some of the pressure loss caused by the addition of the punched baffle. As simulated from reference [16], the pressure loss induced by the baffle is about 400 Pa as its maximum, which is acceptable for a plate-fin heat exchanger. And for the whole plate-fin heat exchanger, the ratio of increased pressure loss is less than 5%. Thus the pressure loss increases not so much for the improved header configuration.

Through qualitatively comparative investigation of above six groups of experimental and numerical results, it can be found that the results of velocity vectors and streamlines between the PIV experiment and numerical simulation are in good agreement with each other. The error between the PIV measurement and numerical simulation is mainly caused by the simplification of physical model and mathematics model in the numerical simulation.

4.3. The comparison of flow distribution of different header configurations

Fig. 15 shows the fluid distribution condition in the axial direction (z-direction) of the three headers, which is at the same inlet Reynolds number ($Re = 6.0 \times 10^4$), where the average outlet velocity for the y-direction is adopted. The fluid distribution is effectively improved for the improved header configuration with punched baffle. The flow maldistribution of the outlet along the header length (z-direction) for configuration A is very serious. The velocities decrease from the axis line to the boundary, they are high in the center part and low in the boundary. Because the flow header has larger dimension comparing to the inlet tube diameter, the fluid tends to go preferentially into the channels in the center. The velocities in the two sides of the header are lower for the fluid has been branched off before it reaches the end of the header. While for the improved header configuration B and configuration C, the velocities adjacent to the two sides are effectively enhanced for the addition of punched baffle, which decrease the velocities near the central axis.

Table 1 illustrates quantitatively the flow maldistribution conditions along the header length (z-direction) of different header configurations. The global flow maldistribution parameter S_g (stated in Eq. (7)) and the ratio of the maximum velocity to the minimum θ (stated in Eq. (8)) of configuration A are large both in the numerical simulation and PIV experiments. While for the improved header configuration with punched baffle, the values decrease obviously. That means the improved header configuration can effectively enhance the flow uniformity in the axial direction (z-direction) of header. And the values of

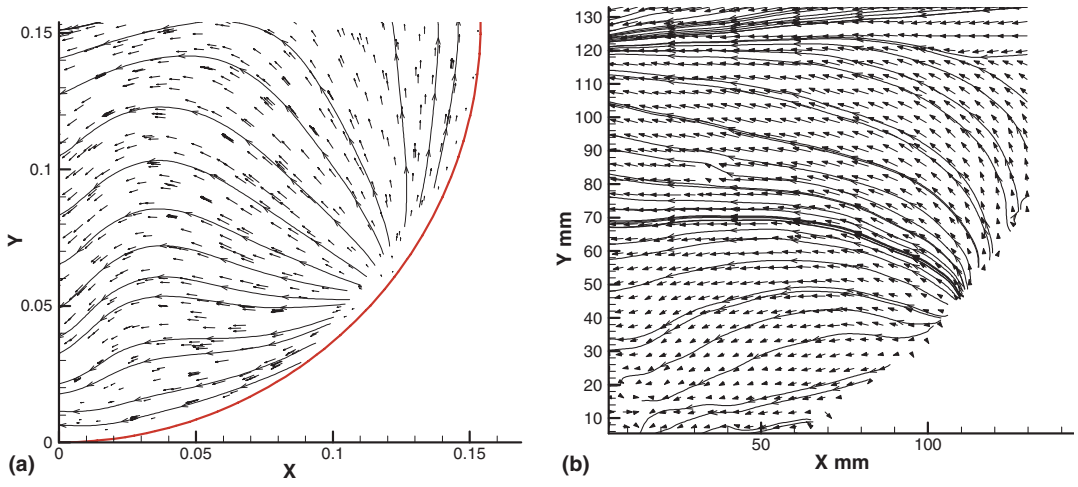

Fig. 14. The velocity vector and streamlines of cross-section 3 (configuration C): (a) CFD results and (b) PIV results.

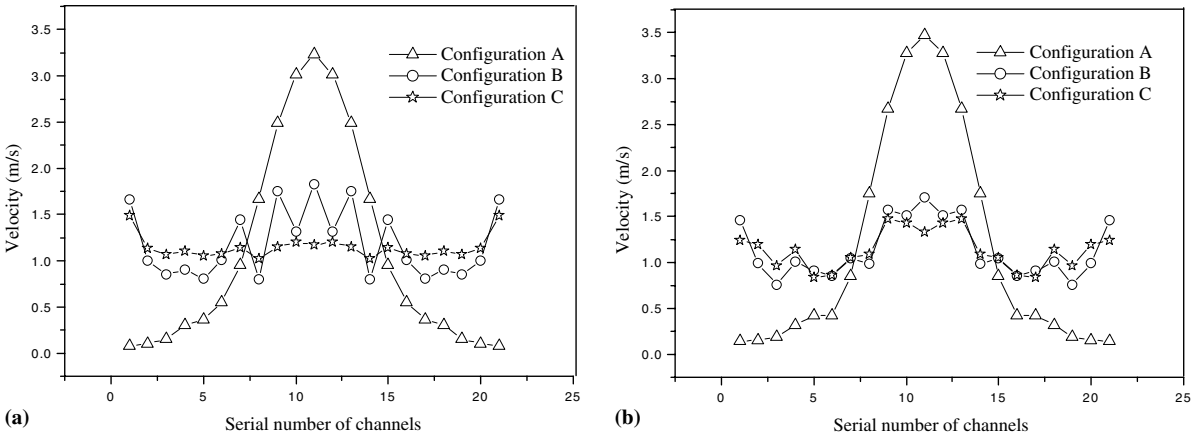

Fig. 15. The velocity distribution along the header length: (a) CFD results and (b) PIV results.

Table 1
S_g and velocity ratio θ of different headers

Maldistribution	Configuration A		Configuration B		Configuration C	
	CFD results	PIV results	CFD results	PIV results	CFD results	PIV results
θ	40.426	23.225	2.287	2.554	1.469	1.763
S_g (m/s)	1.124	1.210	0.371	0.307	0.126	0.209

configuration C is smaller than that of configuration B, which demonstrates that configuration C is predominant than configuration B in the flow field improvement. It is mainly because that configuration C is longer than configuration B and the small holes are distributed in staggered arrangement, which is of great benefit to the flow distribution uniformly. So in the improvement of entrance configuration of plate-fin heat exchanger, configuration C is the first choice.

The fluid distribution condition at the outlet of different cross-sections is illustrated in Table 2. Because the velocities in the two sides of configuration A are lower for the fluid has been branched off before it reaches the end of the header, which is a low-speed zone. So the value of local flow maldistribution parameter S_l of configuration A is smaller than that of configuration B and configuration C at cross-section 3. But at all the other cross-sections, the S_l value of configuration B and configuration C are smaller than that of configuration A, which means that not only in the axial direction but also in the radial direction, the fluid distribution is improved greatly for the improved header configuration with punched baffle. The difference is not so much as that illustrated in Table 1, which is because the physical dimension in radial direction (y-direction) is not so large as that in axial direction (z-direction). It can be concluded from above investigation that it is mainly the header improper configuration that results in the flow maldistribution. So the conventional header configuration A should be improved to enhance the uniformity of flow distribution in plate-fin heat exchangers.

It can be found from the above contrast that the tendency of the numerical simulation results and PIV experimental results are the same and the error is very little. For the conventional header configuration A, it is mainly the difference at inlet velocity that causes the error. In the numerical simulation, it is presumed that the fluid is stable and the velocities of the whole inlet cross-section are equal to each other. While in the practical PIV experiment, the fluid from the upstream fan is not stable for the absence of surge tank and the velocities are not the same. For the improved header configuration with punched baffle, the flow distribution in the axial direction of numerical simulation is more homogeneous than that of PIV experimental. There is also the effect of conduit ferrule that causes the error besides above factors. In the physical model building of numerical simulation, the conduit ferrule is ignored.

Table 2
S_l of different cross-sections

S_l (m/s)	Configuration A		Configuration B		Configuration C	
	CFD results	PIV results	CFD results	PIV results	CFD results	PIV results
Cross-section 1	0.649	0.753	0.363	0.301	0.360	0.312
Cross-section 2	0.712	0.854	0.421	0.363	0.408	0.341
Cross-section 3	0.073	0.134	0.449	0.365	0.457	0.237

While in the PIV experiment, the conduit ferrule exists actually and it may bring some influence to the flow field. But the error may not influence the qualitative investigation for flow field in the entrance configuration of plate-fin heat exchanger.

4.4. The effect of improved header on thermal performance

The objective of the optimization of header configuration is to improve the performance of plate-fin heat exchanger. A further heat transfer experiment was done to show the improvement of the performance of a modular heat exchanger in another experimental table [10]. The experimental system consists of air loop and data acquisition system. The air was supplied by compressor and was divided into two branches. One is heated by electric heater and went into the heat exchanger as the hot fluid. The other directly went into the heat exchanger and exchanged heat energy with the hot fluid. The header configuration of hot fluid was improved (configuration C) and invariable. While that of cold fluid is variable, namely conventional header (configuration A) and improved (configuration C). As shown in Fig. 16, the outlet of cold fluid was divided into 30 paths and was vented into the air after being measured. The data acquisition system consists of sensors, acquisition board, acquisition program and PC. The measurement error of temperature is less than 0.24 °C in the heat transfer experiment.

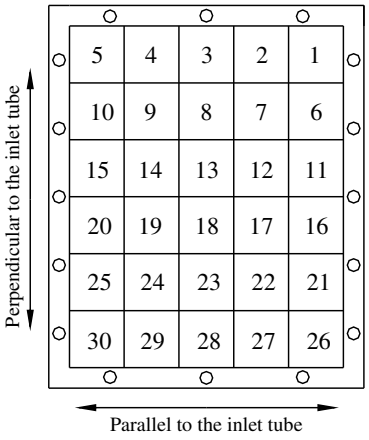

Fig. 16. The division of outlet cross-section for cold fluid.

Fig. 17 shows the outlet temperature distribution of different heat exchangers with different header configurations, which illustrates that the nonuniform distribution of temperature is mainly caused by the fluid maldistribution and the improved header can effectively enhance the efficiency of heat exchanger. The tendency of outlet temperature distribution of different heat exchangers is the same. The high temperatures are located at the center part adjacent to the header inlet tube, the lower are located at the peripheral section. And there is no obvious fluctuation. It is because that the large hot flux of center part exchanges heat with the large cold flux and the small hot flux of peripheral section exchanges heat with the small cold flux. Thus, the temperature distribution does not change too much and the temperature gradient between the center part and the peripheral section is not so large as that of velocity. But at the same inlet conditions ($T_{c,in} = 25$ °C, $T_{h,in} = 50$ °C), there is also obvious difference in the outlet temperature distribution of cold fluid for different header configurations. For the heat exchanger with the conventional header configuration A, the temperature is among the range from 31.72 °C to 35.56 °C, and the average

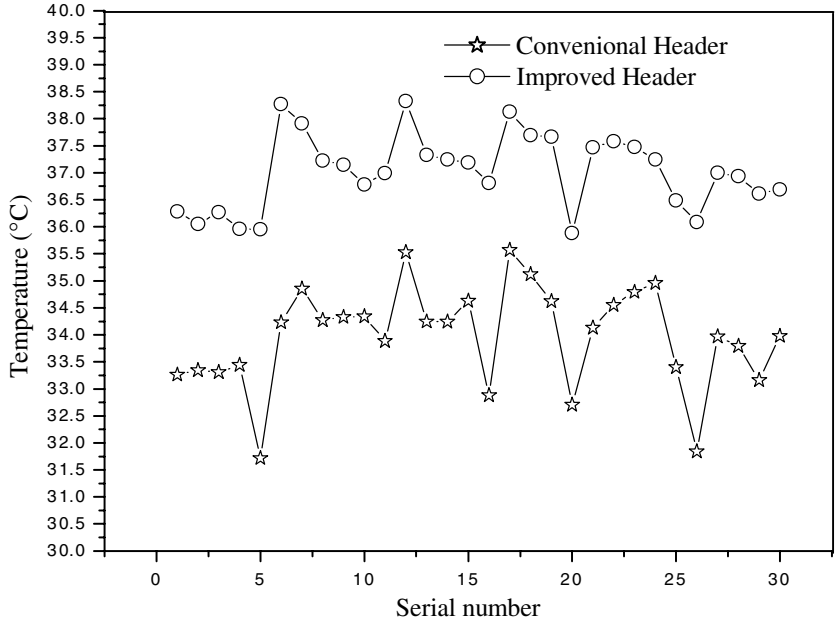

Fig. 17. The outlet temperature distribution of different heat exchangers.

temperature is 33.97 °C. While for that with improved header configuration C, the temperature ranges between 35.88 °C and 38.32 °C, and the average is 37.02 °C. The ratio of the maximum temperature to the minimum is reduced from 1.115 to 1.066. And the heat exchanger efficiency can be enhanced about 12%. So the fluid distribution within the heat exchanger core is more uniform for the header optimization, which results in the temperature uniformly distribution. The more uniformly the fluid is distributed, the more uniformly the energy is distributed. Thus the effective area of heat exchange is made use of sufficiently and heat exchanges homogeneously. So the improvement of header configuration can effectively enhance the efficiency of heat exchange for plate-fin heat exchangers.

5. Conclusions

Flow characteristics of flow field in the entrance of plate-fin heat exchanger have been investigated by means of Particle Image Velocimetry (PIV) and numerical simulation (CFD). The PIV experiment breaks through the shortages of conventional measurement of single point, high workload and so on. The velocity fields were measured using the two-frame cross-correlation technique, which is carried out swiftly, reliably and accurately. The experiments and computations are performed under similar conditions. A series of velocity vector and streamline graphs of different cross-sections are achieved in the PIV experiment and CFD simulation. Both numerical and experimental results indicate that performance of fluid maldistribution in conventional entrance is very serious, while the improved configuration with punched baffle can effectively improve the performance of fluid flow distribution, not only in the radical direction, but also in the axial direction. When the baffle is selected with proper length, the holes are distributed in staggered arrangement, and the punched ratio gradually increases from central axis along with the baffle length, the flow maldistribution parameter S and the velocity ratio θ reduced obviously. The number of vortex decreases compared to that of conventional header configuration and then the energy loss caused by turbulent dissipation reduces. So the pressure loss increases not so much for the improved header configuration. Numerical results and the experimental data are in good agreement with each other. The results validate that PIV and CFD are well suitable to investigate complex flow pattern. The baffle is lower in cost and convenient in assembly, while the effect of the fluid flow distribution uniformly by the improved configuration is obvious. And the improved header can effectively enhance the efficiency of plate-fin heat exchanger and the uniformity of temperature distribution. The conclusion of this paper is of great significance in the improvement of plate-fin heat exchanger.

Acknowledgements

The paper is supported by the Foundation for Excellent Doctoral Dissertation Author by Ministry of Education, and the Doctor Foundation of Xi'an Jiaotong University. The author would like to thank the Ministry of Education, PR China and Xi'an Jiaotong University for their financial support.

References

[1] W.M. Kays, A.L. London, Compact Heat Exchangers, third ed., McGraw-Hill, New York, 1984.
[2] T.F. Yee, I.E. Grossmann, Z. Kravanja, Simultaneous optimization models for heat integration—I. Area and energy targeting and modeling of multi-stream exchangers, Comput. Chem. Eng. 14 (10) (1990) 1151–1164.
[3] B.-D. Chen, Z.-W. Lu, B.-Y. Liu, S.-Z. Lu, in: A Study on Heat Exchanger Network with Multi-fluid Heat Exchanger, Energy and Environment, China Machine Press, Beijing, China, 1998, pp. 313–319.
[4] Ch. Ranganayakulu, K.N. Seetharamu, The combined effect of longitudinal heat conduction, flow nonuniformity and temperature nonuniformity in cross-flow plate-fin heat exchangers, Int. Commun. Heat Mass Transfer 26 (5) (1999) 669–678.
[5] Ch. Ranganayakulu, K.N. Seetharamu, K.V. Sreevatsan, The effects of inlet fluid flow nonuniformity on thermal performance and pressure drops in crossflow plate-fin compact heat exchangers, Int. J. Heat Mass Transfer 40 (1) (1996) 27–38.
[6] R.B. Fleming, The effect of flow distribution in parallel channels of counter-flow heat exchangers, Adv. Cryog. Eng. (12) (1967) 352.
[7] J.P. Chiou, The combined effects of maldistributions of inlet air temperature and the induced flow nonuniformity on the performance of radiator, Heat and Oil Cooler Int. Cong., SAE paper 850037, 1985.
[8] Wilfried Roetzel, Chakkrit Na Ranong, Consideration of maldistribution in heat exchangers using the hyperbolic dispersion model, Chem. Eng. Process. 38 (1999) 675–681.
[9] S. Lalot, P. Florent, S.K. Lang, A.E. Berglles, Flow maldistribution in heat exchangers, Appl. Thermal Eng. 19 (1999) 847–863.
[10] A.J. Jiao, Y.Z. Li, C.Z. Chen, R. Zhang, Experimental investigation on fluid flow maldistribution in plate-fin heat exchanger, Heat Transfer Eng. 24 (4) (2003) 25–31.
[11] Z. Zhang, Y.Z. Li, CFD simulation on inlet configuration of plate-fin heat exchanger, Cryogenics 43 (12) (2003) 673–678.
[12] J. Weterweel, Fundamentals of digital particle image velocimetry, Meas. Sci. Technol. 8 (12) (1997) 1392–1397.
[13] G.R. Duursma, D.H. Glass, S.J.L. Rix, M.I. Yorquez-Ramirez, PIV investigations of flow structures in the fluidised bed freeboard region, Powder Technol. 120 (2001) 2–11.
[14] D. Moreno, F. Mendoza Santoyo, M. Funes-Gallanzi, S. Fernandez Orozco, An optimum velocimetry data display method, Opt. Laser Technol. 32 (2000) 121–128.
[15] Christian Eillert, Markus Raffel, Jurgen Kompenhans, Boleslaw Stasicki, Chistian Kahler, Recent applications of particle image velocimetry in aerodynamic research, Flow Meas. Instrum. 7 (3/4) (1996) 247–256.
[16] Jian Wen, Yanzhong Li, Study of flow distribution and its improvement on the header of plate-fin heat exchanger, Cryogenics 44 (2004) 823–831.
[17] Tao Wenquan, Numerical Heat Transfer, Xi'an Jiaotong University Press, Xi'an, 2002 (in Chinese).
[18] John D. Anderson, Computational Fluid Dynamics, The Basic With Applications, McGraw-Hill Companies, Inc., New York, 1995.